NASA TM X-387

TECHNICAL MEMORANDUM

X-387

EXPERIMENTAL PERFORMANCE OF A HYDROGEN-FLUORINE ROCKET ENGINE AT SEVERAL CHAMBER PRESSURES AND EXHAUST-NOZZLE EXPANSION AREA RATIOS

By William L. Jones, Carl A. Aukerman, and John W. Gibb

Lewis Research Center
Cleveland, Ohio

NATIONAL AERONAUTICS AND SPACE ADMINISTRATION
WASHINGTON
October 1960

NATIONAL AERONAUTICS AND SPACE ADMINISTRATION

TECHNICAL MEMORANDUM X-387

EXPERIMENTAL PERFORMANCE OF A HYDROGEN-FLUORINE ROCKET ENGINE AT SEVERAL CHAMBER PRESSURES AND EXHAUST-NOZZLE EXPANSION AREA RATIOS*

By William L. Jones, Carl A. Aukerman, and John W. Gibb

SUMMARY

The performance of a nominal-5000-pound-thrust liquid-hydrogen - liquid-fluorine rocket engine was evaluated over a range of mixtures from 6 to 20 percent fuel at chamber pressures from 60 to 725 pounds per square inch absolute with exhaust-nozzle area ratios of 3.7, 25, and 100. Performance efficiency near the theoretical maximum (97 percent) and stable operation were obtained over the entire chamber-pressure range at mixtures of 10 to 20 percent fuel.

Performance deficiencies were encountered at mixtures below 10 percent fuel; they were due in part to reduced characteristic velocity and in part to reduced thrust coefficient. The reductions in thrust coefficient were believed to be due to chemical recombination changes in the exhaust nozzle, while reduced characteristic velocity was due to combustion inefficiencies associated with the injector.

The use of rocket ejector devices for altitude simulation was successfully demonstrated in the full-flow operation of the high-area-ratio exhaust nozzles.

INTRODUCTION

Analytical studies indicate that high-energy rocket propellants offer attractive advantages in mission capability over conventional rocket propellants, expecially for upper-atmosphere and space explorations (ref. 1). The propellant combination of hydrogen and fluorine theoretically offers the highest energy potential of all stable chemical rocket propellants. In addition to possessing the highest energy potential, this combination has the advantage over the other promising high-energy combination, hydrogen and oxygen, of requiring a low percentage of

*Title, Unclassified

hydrogen in the propellant. Reduced hydrogen requirements make possible reduced tankage volume and weight. The main disadvantage of fluorine is associated with its extreme reactivity, corrosivity, and toxicity. Nevertheless it has been successfully handled in a number of experimental rocket systems, and satisfactory material and procedure requirements have been established.

The results of an experimental investigation of performance of a hydrogen-fluorine rocket engine at a chamber pressure of 300 pounds per square inch absolute and an area ratio of 3.7 are reported in reference 2. This investigation, conducted at the Lewis Research Center, demonstrated the feasibility of a liquid-hydrogen regeneratively cooled rocket engine and the high performance that can be obtained.

For upper-stage and space vehicles using hydrogen and fluorine, pressurized propellant systems rather than pumped systems are currently receiving favor in the interest of overall system simplicity. This consideration in turn leads to the desirability of low rocket chamber pressures for low-weight tankage and propellant systems. Also of interest for upper-stage and space vehicles are large-expansion-area-ratio exhaust nozzles to take advantage of the potentially high specific impulse. The present investigation was conducted at the Lewis Research Center to determine performance characteristics of a hydrogen-fluorine thrust chamber at low chamber pressures and high area ratios. A range of chamber pressures from 60 to 150 pounds per square inch absolute was investigated with a 3.7 exhaust-nozzle area ratio; exhaust-nozzle area ratios of 3.7 and 25 were investigated at chamber pressures from 200 to 365 pounds per square inch absolute; and a single test was made with a 100 area ratio exhaust nozzle at a chamber pressure of 725 pounds per square inch absolute. Facility limitations prevented obtaining low-chamber-pressure performance with the high-area-ratio exhaust nozzles.

The same basic regeneratively cooled thrust chamber used in reference 2 was used in this investigation; a minor modification provided for increasing the exhaust-nozzle area ratio. The nominal thrust rating for this chamber was 5000 pounds at a chamber pressure of 300 pounds per square inch absolute exhausting to a sea-level atmosphere. A sea-level test facility was used for the investigation. In order to provide full nozzle flow with the high-area-ratio exhaust nozzle at moderate chamber pressures, a zero-flow ejector or exhaust diffuser device was used to reduce the ambient pressure surrounding the nozzle exit. This device utilizes the kinetic energy of the rocket exhaust to create a low-pressure environment surrounding the engine exhaust nozzle.

The symbols used throughout this report, and the methods of calculation of the results are given in appendixes A and B, respectively.

APPARATUS

Facility

The main components of the facility are shown in figure 1. In the schematic drawing the engine and ejector are depicted in relation to the scrubber duct, which is used to remove toxic exhaust products and to reduce the noise. The engine, thrust stand, propellant system, and control room are housed in the building shown on the left in the photograph. Recording instrumentation was located in another building.

Propellant Supply System

Oxidant system. - The fluorine propellant system is shown schematically in figure 2. Liquid nitrogen contained in an open Dewar tank and trough surrounded the fluorine tank, calibrated Venturi flowmeter, control valve, and most of the piping. In this manner the fluorine was maintained in a liquid state and at a constant temperature equal to the normal boiling temperature of nitrogen. Liquid fluorine was desirable both to provide simplified flow control and measurement and to simulate actual vehicle conditions. Helium was used to pressurize the fluorine tank.

Fuel system. - The liquid-hydrogen propellant system is also shown in figure 2. The entire fuel system was insulated with a plastic foam that reduced heat absorption sufficiently to provide a constant temperature in the tank throughout the run. The tank then provided the best location for the hydrogen Venturi flowmeter, since the temperature and pressure, and therefore density, were constant. Gaseous hydrogen was used as the pressurizing and transfer medium.

Engine

Thrust chamber. - The basic chamber used for all runs described herein was designed to produce 5000 pounds of thrust at sea level when operated at a chamber pressure of 300 pounds per square inch absolute. Pertinent geometrical details are:

Chamber characteristic length, L^*, in.	20.4
Chamber contraction area ratio	1.89
Throat area, A_t, sq in.	12
Nozzle divergent conical half-angle, α, deg	15
Nozzle expansion area ratio, ϵ	3.68

The chamber was regeneratively cooled with hydrogen through longitudinal passages of rectangular shape. The passages were formed by a

bundle of longitudinal channels with a ribbon wrapping over the outside. The coolant flow area was established by grinding the channel heights before wrapping to provide for

(1) Local heat-transfer variation

(2) Variation in coolant density from inlet to outlet

(3) Optimum cooling for particular engine operating conditions

Engines designed for 15, 10, and 5 percent fuel at a chamber pressure of 300 pounds per square inch absolute and constructed from nickel were used to obtain the data discussed. Specific details of the design and construction of the engines are described in reference 2. The method used for cooling-passage design is discussed in reference 3.

Nozzles of larger area ratio (25 and 100) were provided by attaching conical nozzle extensions to the basic chamber. These extensions were of a heat-sink design with an expansion half-angle of 15° and depended on a zirconium oxide coating for thermal protection. The length of each run was arbitrarily limited to approximately 15 seconds when these uncooled extensions were used.

Injectors. - The three injectors used in this study are shown in figure 3. The designs included a showerhead, a triplet, and a converging showerhead. The basic pattern or group for each injector was two fuel holes adjacent to each oxidant hole, but additional fuel holes were added around the periphery of the pattern to provide a cooler, fuel-rich region near the chamber walls. The (nonconverging) showerhead and triplet patterns (fig. 3(a)) had identical spacing and were on a flat faceplate. A much finer pattern was used for the converging showerhead (fig. 3(b)) with all holes directed perpendicular to a spherical injector face of 20-inch radius. The number of holes and total flow area for each injector are included in figure 3.

Ejector

With the two large-area-ratio nozzles, altitude simulation was required to expand the exhaust gases in the nozzle fully. This was accomplished by the use of zero-flow ejectors which utilize the kinetic energy of the exhaust jet to reduce the static pressure in the plane of the nozzle exit. Both straight-tube and second-throat ejectors were successfully used. No cooling or thermal protection was needed because of the short run duration. Information from reference 4 was used to design these ejectors, but installation considerations forced compromises, and the following configurations resulted:

Ejector type	Rocket nozzle area ratio	A_{ej}/A_t	A_{ej}/A_{ejt}	L_{ej}/D_{ej}
Straight tube	25	28.0	1.0	9.8
Second throat	25	28.0	1.89	7.05
Second throat	100	107.3	2.19	6.31

The following is a schematic diagram of the engine and ejector installation:

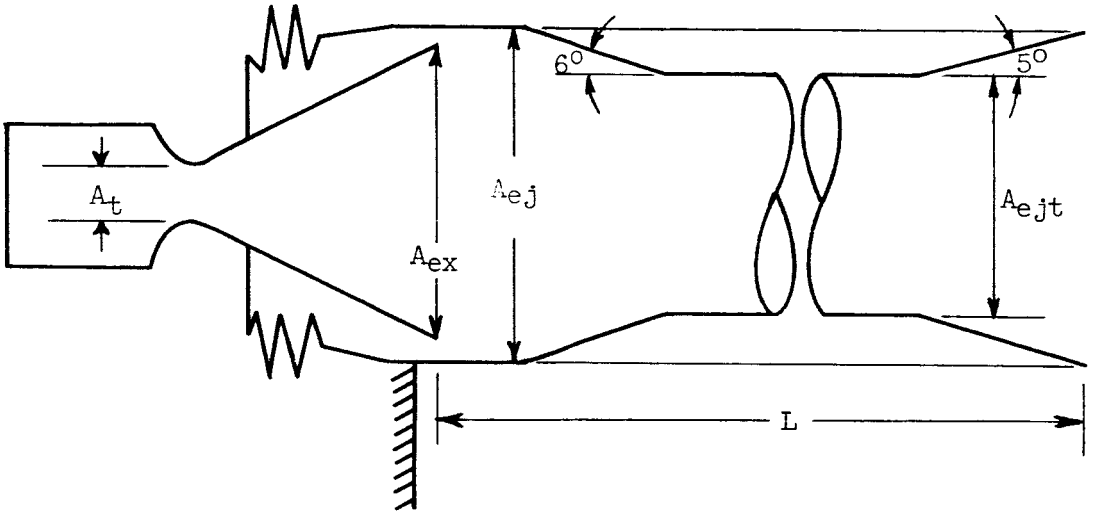

A flexible bellows seal joined the ejector and chamber to make possible force measurements. The calibration procedure and performance calculation involving the bellows seal area are discussed later.

Instrumentation

Locations of all instrumentation are shown in figure 2.

Thrust. - A strain-gage load cell was used for thrust measurement. The signal from the load cell was divided to record on a direct-reading strip chart and on a photographic oscillograph. Prior to each run the load cell was calibrated against a standard load cell. The calibration of the entire thrust system is described in appendix C.

Pressure. - Absolute pressures and pressure differentials were measured with strain-gage-element primary transducers. The pickups were referenced to the atmosphere or a vacuum tank, depending on the range of interest. Signals from the transducers were recorded on direct-reading strip charts and photographic oscillographs. Static calibrations were

made before each run, and probable errors in recorded pressure were approximately 1 percent.

Temperature. - Liquid-hydrogen temperature (40° to 60° R) was measured by carbon resistor elements. The gaseous-hydrogen temperatures (in the injector) were measured by copper-constantan thermocouples, referenced to boiling liquid nitrogen. Direct-reading strip charts were used for temperature recordings.

Control

A closed-loop control system was used to allow presetting of mixture ratios and chamber pressures. Mixture ratio was controlled by feeding the oxidant and fuel Venturi pressure-differential signals to opposite ends of a potentiometer and feeding the output signal to the oxidant-control-valve servomotor. The resulting oxidant-valve movement varied until the potentiometer output was zero. Any desired mixture ratio could be set by proper adjustment of the potentiometer. Several mixture ratios could be included in a single run by switching different potentiometers into the circuit at timed intervals.

Chamber pressure was controlled by comparing the chamber-pressure-transducer output to a predetermined value and feeding the resulting error signal to the fuel-control valve. The resulting change in fuel flow caused the oxidant flow to change, for a constant mixture ratio, and the total-flow adjustment continued until the chamber-pressure-error signal was zero. Step changes or ramps of chamber pressure during a run could be made by mechanically or electrically changing the preset signal. A complete description and an analysis of this system are given in reference 5.

PROCEDURE

Method of Operation

Preparation of the facility for a test program started with thorough cleaning, passivating, and inerting of the fluorine system (ref. 2, p. 17). Then, prior to each run, the thrust measurement system was calibrated (appendix C).

The probability of accumulation of explosive hydrogen-air mixtures in the ejector and scrubber required that the entire system be inerted with carbon dioxide; the oxygen content was monitored to obtain a concentration of less than 3 percent prior to firing of the engine. A continuous carbon dioxide spray during the run maintained a low oxygen level throughout the run.

The operation of the facility during a test run was completely automatic, including engine starting, operation, and shutdown and related safety procedures. A series of timers sequenced the starting as follows:

(1) Recording equipment on

(2) Propellant-systems purge

(3) Water and carbon dioxide sprays in the scrubber duct

(4) Fuel flow lead

(5) Oxidant flow

The run conditions were controlled by the mixture-ratio and chamber-pressure control system described previously with variations programmed as desired. The shutdown procedure was the exact reverse of the starting. Fuel lead and override were necessary to ensure fuel-rich mixtures in the chamber and to provide adequate chamber-wall cooling.

After each period of operation, any large amounts of excess fluorine remaining in the propellant tank were transferred back to the supply trailer; small quantities were disposed of by reaction with carbon using carbon burners (ref. 6). Small amounts of residual hydrogen were allowed to boil off through a remotely located vent.

Engine Starting and Stabilization

A time history of the variation of chamber pressure, thrust, fuel flow, and oxidant flow during a typical run is shown in figure 4. The curves are faired through data taken from oscillograph traces.

Because the propellant combination used is extremely hypergolic, no torch or spark ignition source was necessary. The typical start illustrated in figure 4 included about 2 to 3 seconds for buildup and stabilization of the chamber pressure. A programmed step change in percent fuel is shown at 4.75 seconds followed by about 2 seconds for restabilization of chamber pressure. Following the stabilized portion of the run a ramp decrease in chamber pressure is illustrated. Ramps such as this were programmed to determine pressure ratios during ejector flow breakdown and nozzle flow separation.

The engine performance data reported herein were taken from stabilized portions of similar time plots.

[redacted]

Scope

The range of test conditions investigated with various engine configurations is summarized as follows:

Chamber pressure, P_c, lb/sq in. abs	Percent by weight hydrogen	Nozzle area ratio, ϵ	Injector type
300	6 to 20	3.7	Showerhead and triplet
60 to 150	6 and 10	3.7	Showerhead
200 and 365	6 to 10	25	Showerhead and triplet
725	9	100	Converging showerhead

The choice of chamber pressure for each nozzle was dictated by ejector requirements. The 3.7 area ratio nozzle was designed to flow full at a chamber pressure of 300 pounds per square inch absolute when operated at sea level. The use of a straight-tube ejector enabled test runs to be made down to a chamber pressure of 60 pounds per square inch absolute. The 25 area ratio nozzle required a pressure of 365 pounds per square inch absolute in the chamber to flow full using a straight-tube ejector, but needed only 200 pounds per square inch absolute with a second-throat ejector. A second-throat ejector was also used with the 100 area ratio nozzle.

The first series of test runs was conducted over a range of mixtures from 6 to 20 percent fuel. Inasmuch as the performance increase above 10 percent fuel was small and of lesser interest for vehicle systems using hydrogen because of weight and volume penalties imposed by the low-density fuel, the range of mixtures studied was narrowed to 6 to 10 percent hydrogen in subsequent test runs.

RESULTS

The method of calculation of experimental and theoretical values and adjustments to the theoretical values is described in appendix B. Adjustments have been made throughout the report to values of both frozen- and shifting-equilibrium theoretical impulse for a 15° nonaxial-flow component at the nozzle exit. These adjustments placed the theoretical and experimental data on the same basis inasmuch as all experimental data were obtained with 15° conical exhaust nozzles. Both the experimental data and the corresponding theoretical data are presented in table I. The basic recorded data are presented in table II.

[redacted]

Engine Performance

Effect of mixture ratio. - The variations in c* and c* theoretical equilibrium efficiency with percent fuel for all data obtained within a chamber-pressure range from 200 to 725 pounds per square inch absolute are shown in figure 5. Theoretical equilibrium lines calculated for chamber pressures of 300 and 725 pounds per square inch absolute along with the experimental data are included in figure 5(a). Efficiencies of 97 percent of theoretical equilibrium were obtained with mixtures from about 12 to 20 percent fuel (fig. 5(b)). A drop in c* efficiency from 97 percent to about 94 percent was indicated for the present investigation as the percent fuel was reduced from 12 to 6 percent. The experimental data included from reference 2 indicate lower c* values than the present investigation for mixture ratios corresponding to 10 percent fuel and lower.

The variation of the vacuum thrust coefficient C_F and C_F theoretical equilibrium efficiency with percent fuel is shown in figure 6. Data are shown in figure 6(a) for the two nozzle area ratios of the present investigation and for the 3.7 nozzle from reference 2. The corresponding theoretical equilibrium and frozen data are included. The data from reference 2 for the 3.7 area ratio nozzle indicated equilibrium C_F values throughout the mixture range, while C_F values for the 25 area ratio nozzle of the present investigation indicate a decided reduction in C_F at mixtures below about 10 percent fuel. The single data point at the 100 area ratio and about 9 percent fuel fell on the theoretical equilibrium line.

The C_F efficiencies for all three nozzle area ratios are shown in figure 6(b). Data from the present investigation indicate a drop in C_F efficiency to about 95 percent as the percent fuel was reduced to about 6. At mixtures above 10 percent fuel values of C_F higher than theoretical may have resulted from the assumptions made in obtaining and using nozzle-inlet pressure in the calculation of C_F (see appendix B).

Vacuum specific impulse and theoretical equilibrium impulse efficiency are presented in figure 7 as a function of percent fuel. Data from the present investigation as well as from reference 2 are included. The theoretical equilibrium and frozen data corresponding to the three nozzle area ratios are included in figure 7(a) for comparison. Both the 25 area ratio data of the present investigation and the 3.7 area ratio data of reference 2 show the same decreasing impulse toward the theoretical frozen performance line as the percent fuel was reduced from about 12 to 6. The vacuum specific impulse efficiency is presented as a function of percent fuel in figure 7(b). About 98 percent efficiency is shown for mixtures between 11 and 20 percent fuel. At mixtures of about 6 percent fuel the impulse efficiency decreased to about 91 percent. The single data point obtained with the 100 area ratio exhaust nozzle at

about 9 percent fuel and a chamber pressure of 725 pounds per square inch absolute coincided with the theoretical equilibrium value. The fact that the performance was slightly higher for this run than for runs with the 3.7 and 25 area ratio nozzles may have been due to the use of a different injector type, which incorporated a converging jet showerhead (fig. 3(b)) that contained about two times as many oxidant holes as the injectors used with the other exhaust-nozzle area ratios.

Effect of chamber-pressure variation. - Inasmuch as the present investigation was conducted in a sea-level test facility, it was not possible to obtain performance at low values of chamber pressure, while maintaining full nozzle flow, for either the 25 or 100 exhaust-nozzle area ratio configurations. Therefore the investigation at low values of chamber pressure (60 to 150 lb/sq in. abs) was conducted with the 3.7 area ratio nozzle only. By use of the zero-flow ejector it was possible to operate with the 3.7 area ratio nozzle flowing full down to the minimum chamber pressure of the investigation (from 150 to 60 lb/sq in. abs). The chamber and injector configurations were the same as those used for the investigation of reference 2.

The effects of chamber-pressure variation on the c* performance for 10 percent fuel are shown in figure 8. The increase in c* and c* efficiency obtained with decreasing chamber pressure may be the result of better propellant vaporization. References 7 and 8 show that better propellant vaporization in the rocket chamber can result if the difference between the two propellant injection velocities is increased. Calculation of the propellant injection velocities indicated that a ΔV, $V_{H_2} - V_{F_2}$, increase of about 40 percent resulted as the chamber pressure was reduced from 365 to 60 pounds per square inch absolute. This increase in ΔV at the low chamber pressures was primarily due to increased hydrogen injection velocity resulting from lower hydrogen density at the lower pressures and higher injection temperatures associated with the higher coolant temperatures.

The effect of variation in chamber pressure on the vacuum specific impulse for 10 percent fuel is presented in figure 9. The trend of the data toward higher impulse performance at the lower values of chamber pressure is believed to be a primary result of the improved c* efficiency previously discussed (fig. 8).

Effect of exhaust-nozzle area ratio. - The variation of vacuum specific impulse with exhaust-nozzle area ratio is illustrated in figure 10. The data for this illustration were taken from figure 7(a) for values of nozzle area ratio of 3.7, 25, and 100. Curves of theoretical equilibrium and frozen flow are included for comparison. Experimental values were very near the theoretical equilibrium values for all nozzle area ratios.

Exhaust-nozzle performance. - The ratio of rocket chamber pressure to nozzle wall pressure at several stations throughout the 25 area ratio exhaust nozzle for three values of percent fuel is shown in figure 11. Two equilibrium-expansion-flow lines and one frozen-expansion-flow line are included for comparison. The pressures throughout the nozzle were generally very near the equilibrium values. At the larger values of area ratio an effect of variation in percent fuel is apparent. As percent fuel is decreased the chamber- to nozzle-pressure ratio increases toward the frozen-flow curve.

Figure 12 presents the exhaust-nozzle pressure ratio for the 25 area ratio exhaust nozzle as a function of percent fuel. Curves for both theoretical-frozen and equilibrium nozzle-expansion performance are included for comparison. The experimental data show a trend away from the equilibrium and toward the frozen performance line as mixture ratio is reduced below about 10 percent fuel. This trend toward the frozen performance is similar to the trend in C_F (fig. 6).

Regenerative Cooling Characteristics

Except for the uncooled nozzle extensions used in the 25 and the 100 nozzle area ratio tests the entire thrust chamber was regeneratively cooled with the liquid-hydrogen fuel. The fuel entered the chamber at the downstream end and traveled through the rectangular-shaped cooling passages into the injector. As noted in the sections APPARATUS and PROCEDURE, chambers having different cooling-passage designs based on operation at mixtures of 5, 10, and 15 percent fuel were used for the investigation. Coolant temperature rise obtained over a range of chamber pressures and percent fuels is illustrated in figure 13. The experimental data are distinguished only as low-chamber-pressure (60 to 200 lb/sq in. abs) or high-chamber-pressure (300 to 725 lb/sq in. abs) data. Two calculated theoretical lines are shown based on a chamber pressure of 300 pounds per square inch absolute with 10 percent fuel assuming (1) 100 percent c* efficiency and (2) the experimental c* efficiency. A third calculated theoretical curve is also included based on a chamber pressure of 60 pounds per square inch absolute, 10 percent fuel, and 100 percent c* efficiency. These curves were calculated using the method given in reference 3. No distinction is made in the experimental data between chambers having different cooling-passage designs, since no particular trend was evident; nevertheless, the operating metal temperatures of the cooling passages would be affected by the passage design.

The significant result illustrated by the data in this figure is the close agreement in trend of the experimental and the calculated coolant temperature rise. Some trend toward higher values of ΔT is indicated by both the experimental and the calculated data at low chamber pressure.

[redacted]

DISCUSSION

Although very high vacuum-specific-impulse performance was obtained at mixture ratios corresponding to 10 percent fuel and higher, considerably reduced performance occurred at lower values of percent fuel. The reduced impulse performance was found to be the same for the present investigation as for the investigation of reference 2; however, the individual parameters for c^* and C_F of this investigation are not in agreement with those in reference 2. The additional data obtained from the present investigation result in a change in fairing of both c^* and C_F efficiency curves at the lower values of percent fuel (figs. 5 and 6). The fairing of the C_F efficiency curve herein is in agreement with the exhaust-nozzle pressure-ratio data (fig. 12). Inasmuch as nozzle pressure ratio is directly related to C_F for a given mixture ratio and nozzle area ratio, the trend of this parameter with mixture ratio affords an independent check of the trend of C_F observed in the present investigation.

Although both aerodynamic and chemical kinetic effects could cause deficiencies in C_F, it is unlikely that the aerodynamic characteristics would change perceptibly with changes in mixture ratio. The chemical kinetic effects of dissociation in the rocket chamber and recombination in the rocket exhaust nozzle, however, would be expected to be influenced by mixture ratio.

The change in fairing of the c^* curve was a result of utilizing more extensive data obtained at low percent fuel in the present investigation. This fairing of the c^* efficiency curve also was required to satisfy the relation $Ig_c = c^*C_F$.

From the results obtained in the present investigation the deficiency in impulse performance at mixture ratios corresponding to low percent fuel was due in part to combustion inefficiency associated with the injector and in part to chemical kinetic effects in the nozzle. Of the 7 to 8 percentage points of deficiency in impulse performance, the data herein indicate 4 to $4\frac{1}{2}$ to be in C_F and 3 to $3\frac{1}{2}$ in c^*.

Another result indicated by comparing data of reference 2 with data of the present investigation is the effect of nozzle area ratio. Figure 7(b) shows data obtained with both 3.7 (ref. 2) and 25 nozzle area ratios. The experimental data shown in the figure indicate no effect of nozzle area on impulse efficiency. The single data point with the 100 nozzle area ratio, although indicating a higher level of impulse performance, has about the same C_F performance as the two other nozzles but a higher value of c^* efficiency.

[redacted]

SUMMARY OF RESULTS

The results obtained from an experimental investigation of the performance of a hydrogen and fluorine rocket engine at several chamber pressures and exhaust-nozzle area ratios are summarized as follows:

1. Performance values of 97 percent of the theoretical maximum were obtained for both specific impulse and characteristic velocity at chamber pressures of about 300 pounds per square inch absolute and mixtures from 12 to 20 percent fuel.

2. Performance at chamber pressures of about 300 pounds per square inch absolute decreased as the percent fuel was reduced below 12. At 6 percent fuel specific impulse was about 91 percent of the theoretical maximum, while characteristic velocity and thrust coefficient were down to 94 and 95 percent, respectively. The lower performance values at the lower percent fuel indicated research problem areas both in combustion efficiency and in exhaust-nozzle chemical recombination effects.

3. Stable operation as well as high performance (near 100 percent) were obtained at the low chamber pressures (60 to 150 lb/sq in. abs).

4. Nearly 100 percent of maximum theoretical performance was obtained with an exhaust-nozzle area ratio of 100 at 9 percent fuel and a chamber pressure of 725 pounds per square inch absolute.

5. The experimental data indicate no effect of nozzle area ratio on impulse efficiency (experimental vacuum specific impulse/theoretical equilibrium vacuum specific impulse).

6. An exhaust ejector was successfully used to provide altitude simulation for exhaust-nozzle area ratios up to 100.

Lewis Research Center
National Aeronautics and Space Administration
Cleveland, Ohio, June 22, 1960

[redacted]

APPENDIX A

SYMBOLS

A area, sq in.

C_F thrust coefficient

c* characteristic velocity, ft/sec

D diameter

F thrust, lb

g_c gravitational conversion factor, $32.2 \frac{\text{ft-lb mass}}{(\text{sec}^2)(\text{lb force})}$

I specific impulse, lb-sec/lb

L length, in.

L* characteristic length, chamber volume/throat area, in.

$\dot{m}$ mass flow, $\dot{w}/g_c$

P absolute pressure, total unless otherwise indicated

ΔT temperature change, ^{o}R

V velocity, ft/sec

V_i resultant injection velocity, $\frac{(\dot{w}V)_{H_2} + (\dot{w}V)_{F_2}}{\dot{w}_{H_2} + \dot{w}_{F_2}}$

$\dot{w}$ propellant weight flow, lb/sec

α half-angle of nozzle divergence

ϵ nozzle expansion area ratio, A_{ex}/A_t

λ nozzle divergence correction factor, $(1 + \cos \alpha)/2$

Subscripts:

a ambient

b flexible bellows seal joint

[redacted]

c	combustion chamber
ej	ejector
ejt	ejector throat
eq	equilibrium theoretical
ex	nozzle exit
F_2	fluorine or fluorine propellant system
fr	frozen theoretical
H_2	hydrogen or hydrogen propellant system
i	injector
m	measured
n	nozzle entrance
s	static
t	nozzle throat
vac	vacuum
x	experimental

APPENDIX B

PERFORMANCE CALCULATIONS

Theoretical

Theoretical performance data were taken from reference 9. Calculations from reference 9 were based on the following assumptions: perfect gas law, frictionless flow, homogeneous mixing, adiabatic combustion at constant pressure (nozzle-inlet total pressure), isentropic expansion, ambient pressure equal to zero, one-dimensional flow, adjustments to theoretical calculations corrected for a finite chamber contraction area ratio, and a 15° half-angle exhaust nozzle.

Characteristic velocity. - Characteristic velocity, based on nozzle-inlet total pressure, is

$$c_n^* = \frac{P_{c,n} A_t g_c}{\dot{w}} \tag{1}$$

Vacuum specific impulse. - The general rocket thrust equation with divergent exhaust flow is

$$F = \dot{m}_{ex} V_{ex} \lambda + (P_{ex} - P_a) A_{ex} \tag{2}$$

When vacuum performance is desired, P_a becomes zero and

$$F_{vac} = \dot{m}_{ex} V_{ex} \lambda + P_{ex} A_{ex} \tag{3}$$

Since $I = F/\dot{w}$, the theoretical vacuum impulse for an engine is

$$I_{vac} = \frac{F_{vac}}{\dot{w}} = \frac{\dot{m} V_{ex} \lambda}{\dot{w}} + \frac{P_{ex} A_{ex}}{\dot{w}}$$

$$I_{vac} = I\lambda + \frac{P_{ex} A_{ex}}{\dot{w}}$$

Theoretical calculations, being generalized, do not specify $\dot{w}$ but give values of I and c_n^*. It is therefore convenient to express $\dot{w}$ in terms of c_n^* in the preceding equation:

$$I_{vac} = I\lambda + \frac{c_n^* \epsilon P_{ex}}{g_c P_{c,n}} \tag{4}$$

Vacuum thrust coefficient. - Having defined vacuum thrust and vacuum impulse, the nozzle vacuum thrust coefficient C_F becomes

$$C_{F,vac} = \frac{F_{vac}}{A_t P_{c,n}} = \frac{I_{vac} g_c}{c_n^*} \tag{5}$$

Experimental

Chamber pressure. - Theoretical calculations are based on the total pressure of the combustion gases at the entrance to the nozzle $P_{c,n}$; but in this program, it was more convenient to measure the pressure at the injector $P_{c,i}$, where combustion gas velocity may be considered negligible. The loss in total pressure between the two stations was that required to accelerate the gases to nozzle-inlet velocity in a constant-area chamber. The following equation is derived in reference 10 (p. 17) assuming that pressures are radially uniform, flow is frictionless, and combustion is completed at the nozzle entrance:

$$\frac{P_{c,i}}{P_{c,n,x}} = \left(\frac{P_{c,n,s}}{P_{c,n}}\right) + \frac{I_n g_c - V_i}{c_n^*(A_c/A_t)} \tag{6}$$

Solving for $P_{c,n,x}$

$$P_{c,n,x} = \frac{P_{c,i}}{\left(\frac{P_{c,n,s}}{P_{c,n}}\right) + \frac{I_n g_c - V_i}{c_n^*(A_c/A_t)}} \tag{7}$$

Characteristic velocity. - The experimental characteristic velocity was then based on this corrected nozzle-inlet total pressure using the equation

$$c_{n,x}^* = \frac{P_{c,n,x} A_t g_c}{\dot{w}} \tag{8}$$

Specific impulse. - A force balance on the engine and ejector system in the axial direction is required to determine vacuum thrust and impulse experimentally.

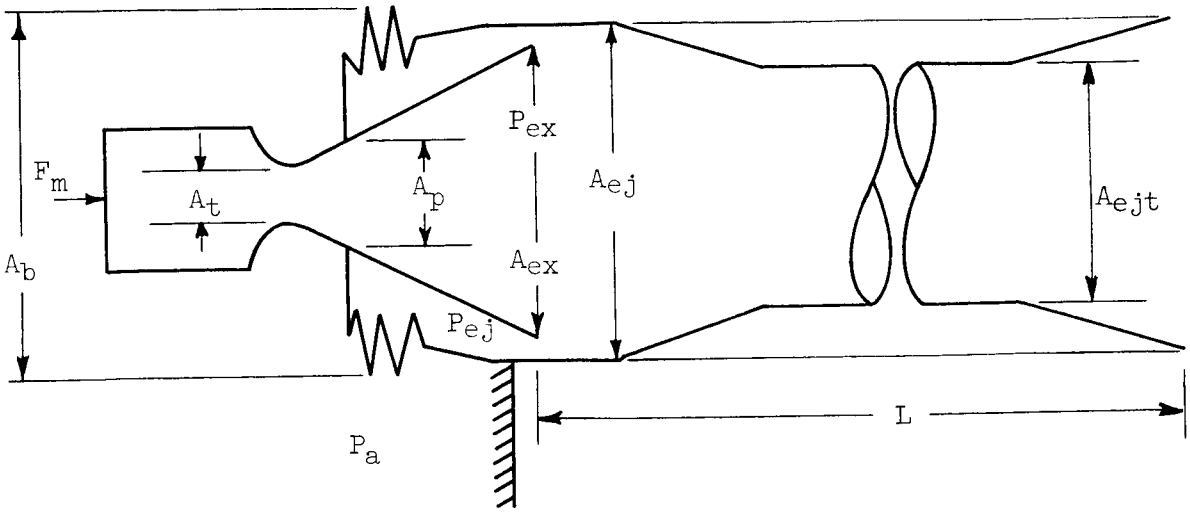

The summation of all forces (see diagram above) gives

$$F_m = \dot{m}_{ex}V_{ex}\lambda + P_{ex}A_{ex} + P_{ej}(A_b - A_p) - P_aA_b - P_{ej}(A_{ex} - A_p)$$

Using equation (3) for vacuum thrust and eliminating the term $\dot{m}_{ex}V_{ex}\lambda$, the total vacuum thrust for the system is found to be

$$F_{vac,x} = F_m + A_{ex}P_{ej} + A_b(P_a - P_{ej}) \tag{9}$$

where F_m is thrust measured by the load cell, $A_{ex}P_{ej}$ is vacuum thrust addition, and $A_b(P_a - P_{ej})$ is bellows seal force. The experimental vacuum specific impulse is

$$I_{vac,x} = \frac{F_{vac,x}}{\dot{w}} \tag{10}$$

Vacuum thrust coefficient. - Vacuum thrust and nozzle-inlet total pressure were used to define vacuum thrust coefficient as follows:

$$C_{F,vac,x} = \frac{F_{vac,x}}{P_{c,n,x}A_t} = \frac{I_{vac}g_c}{c^*_{n,x}} \tag{11}$$

E-636

CG-3 back

APPENDIX C

THRUST CALIBRATION

The equation for total vacuum thrust, as derived in appendix B for this facility, is

$$F_{vac} = F_m + A_b(P_a - P_{ej}) + A_{ex}P_{ej}$$

Each term in this equation is a variable and had to be included in the calibration procedure except the nozzle-exit area A_{ex} and the ambient pressure P_a. The procedure for calibration of the thrust load cell and effective seal area was as follows:

(1) The ejector tube was temporarily sealed at the exit.

(2) An axial force was applied to the thrust stand by an air cylinder whose output was measured by a standard calibrating load cell. In this manner the primary thrust load cell was calibrated as the applied force was increased to the maximum expected load.

(3) While holding a constant force on the calibrating load cell, the ejector tube was evacuated, in step fashion, to approximately 0.2 pound per square inch absolute. At each recorded pressure a different load on the primary thrust load cell was also recorded. The effective seal area was then calculated from the relation

$$\Delta F = A_b \Delta P$$

where ΔF is change in load cell output due to ejector evacuation, A_b is effective seal area, and ΔP is difference between evacuated ejector pressure and ambient.

The ejector- and nozzle-pressure pickups were also calibrated during the evacuation process. For a complete calibration, the applied load was reduced in a series of steps at full vacuum and the entire procedure was repeated in reverse.

The probable accuracy of the total-thrust measurement was approximately 1 percent.

REFERENCES

1. Henneberry, H. M., Moseson, M. L., and Himmel, S. C.: Comparison of High Energy Propellants in Final Stages. Paper presented at Inst. Aero. Sci. Meeting, Cleveland (Ohio), Mar. 1959. (ASTIA No. AD 305988.)

2. Douglass, H. W., Hennings, G., and Price, H. G., Jr.: Experimental Performance of Liquid Hydrogen and Liquid Fluorine in Regeneratively Cooled Rocket Engines. NASA TM X-87, 1959.

3. Curren, Arthur N., Price, Harold G., Jr., and Douglass, Howard W.: Analysis of Effects of Rocket-Engine Design Parameters on the Regenerative-Cooling Capabilities of Several Propellants. NASA TN D-66, 1959.

4. Jones, William L., Price, Harold G., Jr., and Lorenzo, Carl F.: Experimental Study of Zero-Flow Ejectors Using Gaseous Nitrogen. NASA TN D-203, 1960.

5. Otto, Edward W., and Flage, Richard A.: Control of Combustion-Chamber Pressure and Oxidant-Fuel Ratio for a Regeneratively Cooled Hydrogen-Fluorine Rocket Engine. NASA TN D-82, 1959.

6. Schmidt, Harold W.: Reaction of Fluorine with Carbon as a Means of Fluorine Disposal. NACA RM E57E02, 1957.

7. Ingebo, Robert D.: Drop-Size Distributions for Impinging-Jet Breakup in Airstreams Simulating the Velocity Conditions in Rocket Combustors. NACA TN 4222, 1958.

8. Clark, Bruce J., Hersch, Martin, and Priem, Richard J.: Propellant Vaporization as a Criterion for Rocket-Engine Design; Experimental Performance, Vaporization, and Heat-Transfer Rates with Various Propellant Combinations. NASA MEMO 12-29-58E, 1959.

9. Fortini, Anthony, and Huff, Vearl N.: Theoretical Performance of Liquid Hydrogen and Liquid Fluorine as a Rocket Propellant for a Chamber Pressure of 600 Pounds per Square Inch Absolute. NACA RM E56L10a, 1957.

10. Huff, Vearl N., Fortini, Anthony, and Gordon, Sanford: Theoretical Performance of JP-4 Fuel and Liquid Oxygen as a Rocket Propellant. II - Equilibrium Composition. NACA RM E56D23, 1956.

TABLE I. - REGENERATIVELY COOLED ROCKET ENGINE PERFORMANCE WITH LIQUID HYDROGEN AND LIQUID FLUORINE

Injector type	Nozzle area ratio, ϵ	Nozzle throat area, A_t, sq in.	Experimental values								Theoretical values					Experimental efficiency		
			Chamber pressure, $P_{c,n,x}$, lb/sq in. abs	Mixture ratio		Total propellant flow rate, w, lb/sec	Total vacuum thrust, $F_{vac,x}$, lb	Vacuum specific impulse, $I_{vac,x}$, lb-sec/lb	Characteristic velocity, $c^*_{n,x}$, ft/sec	Vacuum thrust coefficient, $C_{F,vac,x}$	Vacuum specific impulse, I_{vac}, lb-sec/lb		Characteristic velocity, $c^*_{n,eq}$, ft/sec	Vacuum thrust coefficient, $C_{F,vac}$		$\frac{I_{vac,x}}{I_{vac,eq}}$	$\frac{c^*_{n,x}}{c^*_{n,eq}}$	$\frac{C_{F,vac,x}}{C_{F,vac,eq}}$
				Percent hydrogen	Oxidant-fuel ratio						Equilibrium	Frozen		Equilibrium	Frozen	×100	×100	×100
Showerhead[a]	3.68	12.155	366.0	18.97	4.27	17.20	6,687	388.8	8320	1.505	401.6	395.1	8404	1.539	1.523	96.8	99.0	97.8
			289.0	19.63	4.09	14.07	5,500	390.9	8037	1.566	400.5	394.6	8389	1.537	1.537	97.6	95.8	101.9
			289.0	15.78	5.34	13.90	5,500	395.7	8127	1.568	404.2	391.2	8404	1.549	1.538	97.9	96.7	101.2
			288.0	11.66	7.58	14.01	5,507	393.1	8046	1.573	402.1	381.5	8269	1.566	1.537	97.8	97.3	100.5
			308.0	10.80	8.26	15.00	5,832	388.8	8035	1.558	401.0	379.3	8233	1.568	1.537	97.0	97.6	99.5
			307.0	8.95	10.17	15.21	5,833	383.5	7898	1.564	397.2	373.3	8134	1.572	1.536	96.6	97.1	99.5
			305.0	7.02	13.25	15.85	5,788	365.2	7533	1.561	392.1	365.0	8014	1.575	1.534	93.1	94.0	99.0
Triplet[a]	3.68	12.007	300.0	13.79	6.26	14.24	5,648	396.6	8125	1.572	405.3	388.2	8359	1.561	1.541	97.9	97.2	100.7
			300.0	9.78	9.23	14.73	5,684	385.9	7857	1.582	400.0	376.7	8176	1.575	1.540	96.5	96.1	100.3
			296.0	7.96	11.56	14.96	5,589	373.6	7629	1.577	395.6	370.1	8073	1.578	1.538	94.4	94.5	100.0
			298.0	6.12	15.34	16.06	5,677	353.5	7165	1.586	389.5	359.6	7917	1.584	1.537	90.8	90.5	100.2
Showerhead	3.61	12.10	142.1	9.97	9.03	6.80	2,695	396.3	8141	1.566	395.6	370.6	8110	1.571	1.532	100.2	100.4	99.7
			100.5	9.94	9.06	4.80	1,904	396.7	8155	1.568	394.5	368.2	8070	1.574	1.532	100.6	101.0	99.5
			81.3	9.95	9.05	3.93	1,536	390.8	8060	1.561	392.6	367.0	8050	1.571	1.533	99.5	100.1	99.4
			80.3	10.00	9.00	2.90	1,134	391.0	8100	1.554	392.0	364.6	8020	1.575	1.532	99.7	101.0	98.7
Showerhead	3.69	11.85	140.4	5.77	16.33	7.00	2,648	378	7650	1.591	382.8	351	7750	1.591	1.536	98.7	98.7	100.0
			100.4	5.70	16.54	5.27	1,887	358	7280	1.583	381.2	348	7710	1.592	1.534	93.9	94.4	99.4
Showerhead	25	12.155	369.3	9.79	9.22	18.30	8,149	445.2	7897	1.815	458.8	417.7	8195	1.801	1.700	97.0	96.4	100.8
		12.007	368.7	10.17	8.83	18.13	8,086	446.0	7866	1.824	459.1	419.3	8215	1.798	1.701	97.1	95.8	101.4
			367.9	8.14	11.29	18.45	8,087	438.3	7711	1.829	458.2	410.5	8100	1.820	1.697	95.7	95.2	100.5
		12.007	374.0	10.03	8.97	18.31	8,260	451.1	7800	1.861	459.2	419.0	8210	1.799	1.702	98.2	95.0	103.4
Triplet	25	12.024	365.6	7.83	11.77	18.08	7,798	431.4	7831	1.774	457.9	408.9	8080	1.823	1.697	94.2	96.9	97.3
			366.7	5.94	15.84	19.04	7,740	406.5	7457	1.754	453.8	395.0	7895	1.849	1.691	89.5	94.4	94.9
		12.024	201.3	7.50	12.33	9.97	4,317	433.0	7817	1.782	455.5	401.6	7990	1.834	1.692	95.1	97.8	97.2
			201.1	5.56	16.99	10.62	4,269	402.0	7345	1.761	449.5	385.2	7755	1.865	1.687	89.4	94.7	94.4
Converging showerhead	100	12.024	725.0	8.86	10.29	34.23	16,495	481.9	8205	1.893	481.2	436	8200	1.891	1.77	100.1	100.0	100.1

[a]Runs originally reported in ref. 2.

TABLE II. - BASIC PARAMETERS AND RECORDED DATA FOR REGENERATIVELY COOLED ROCKET ENGINE WITH LIQUID HYDROGEN AND LIQUID FLUORINE

Thrust components			Momentum correction, $P_{c,i}/P_{c,n}$	Ejector pressure, P_{ej}, lb/sq in. abs	Seal pressure, P_b, lb/sq in. abs	Injector face chamber pressure, $P_{c,i}$, lb/sq in. abs	Hydrogen injector pressure drop, $\Delta P_{H_2,i}$, lb/sq in. abs	Hydrogen coolant-passage pressure drop, $\Delta P_{coolant}$, lb/sq in. abs	Fluorine injector pressure drop, $\Delta P_{F_2,i}$, lb/sq in. abs	Hydrogen coolant-passage temperature rise, $\Delta T_{coolant}$, °R (a)	Hydrogen injection velocity, V_{H_2}, ft/sec	Fluorine injection velocity, V_{F_2}, ft/sec	Nozzle wall static pressure, lb/sq in. abs					
Measured thrust, F_m, lb	Bellows seal thrust, $A_b(P_a - P_{ej})$, lb	Vacuum thrust addition, $A_{ex}P_{ej}$, lb											Expansion area ratio, ϵ					
													3.7	6.6	10	14.2	19.2	25
6,050	----	638	1.0439	14.47	-----	382.3	65	129	---	145	1365	110	-----	----	-----	----	----	----
4,865	----	633	1.0429	14.34	-----	301.7	39	89	---	151	1436	95	-----	----	-----	----	----	----
4,870	----	633	1.0437	14.34	-----	301.7	36	82	---	222	1615	98	-----	----	-----	----	----	----
4,674	----	633	1.0458	14.34	-----	301.5	29	71	---	321	1660	104	-----	----	-----	----	----	----
5,201	----	630	1.0442	14.29	-----	322.0	28	84	---	400	2020	112	-----	----	-----	----	----	----
5,201	----	630	1.0454	14.29	-----	321.0	23	70	---	480	1980	116	-----	----	-----	----	----	----
5,158	----	630	1.0457	14.29	-----	319.3	17	62	---	574	1960	124	-----	----	-----	----	----	----
5,013	----	637	1.0430	14.25	-----	312.4	79	138	---	313	1960	103	-----	----	-----	----	----	----
5,047	----	637	1.0446	14.25	-----	313.0	65	110	---	483	2100	112	-----	----	-----	----	----	----
4,952	----	637	1.0475	14.25	-----	309.6	52	96	---	638	2030	116	-----	----	-----	----	----	----
5,040	----	637	1.0455	14.25	-----	311.4	22	67	---	660	1965	117	-----	----	-----	----	----	----
1,848	884	265	1.045	6.08	6.08	148.3	26	46	57	384	1526	51	-----	----	-----	----	----	----
995	736	173	1.040	3.95	3.95	104.5	29	33	35	474	1800	36	-----	----	-----	----	----	----
599	810	127	1.039	2.90	2.90	84.5	29	27	25	545	2042	30	-----	----	-----	----	----	----
186	842	106	1.036	2.44	2.44	63.0	20	19	16	530	1980	23	-----	----	-----	----	----	----
1,690	825	133	1.046	3.06	3.06	147	13	42	35	808	1757	55	7.2	----	-----	----	----	----
902	691	94	1.042	2.16	2.16	105	9	38	23	940	2115	41	4.7	----	-----	----	----	----
6,326	1570	250	1.0444	0.828	-----	385.7	88	109	279	412	1562	139	19.0	7.15	4.00	2.82	2.04	1.28
6,244	1654	185	1.0440	0.596	0.635	384.9	86	143	257	392	1540	137	14.35	7.00	3.91	2.65	1.75	1.00
6,248	1653	187	1.0462	0.596	0.645	384.9	78	113	284	485	1529	142	14.35	6.85	3.91	2.75	1.75	1.00
6,363	1642	254	1.0440	0.865	0.818	390.4	83	140	257	415	1596	138	15.38	8.41	4.59	3.00	1.95	1.15
5,916	1665	218	1.0469	0.732	0.715	382.7	45	291	292	468	1502	140	-----	8.45	4.65	2.95	1.87	1.05
5,853	1667	215	1.0471	0.722	0.699	384.0	36	254	330	640	1603	150	-----	7.60	4.35	2.70	1.75	.95
2,490	1669	158	1.0501	0.507	0.539	211.4	30	168	82	652	1939	77	-----	4.25	3.42	1.84	1.10	.55
2,446	1673	149	1.0515	0.479	0.508	211.4	22	142	99	584	2081	84	-----	3.95	3.17	1.50	1.00	.50
14,421	1563	511	1.041	0.425	0.360	756.0	109	433	338	685	1775	127	-----	----	10.2	7.1	4.3	----

[a]Based on constant coolant inlet temperature of 50° R.

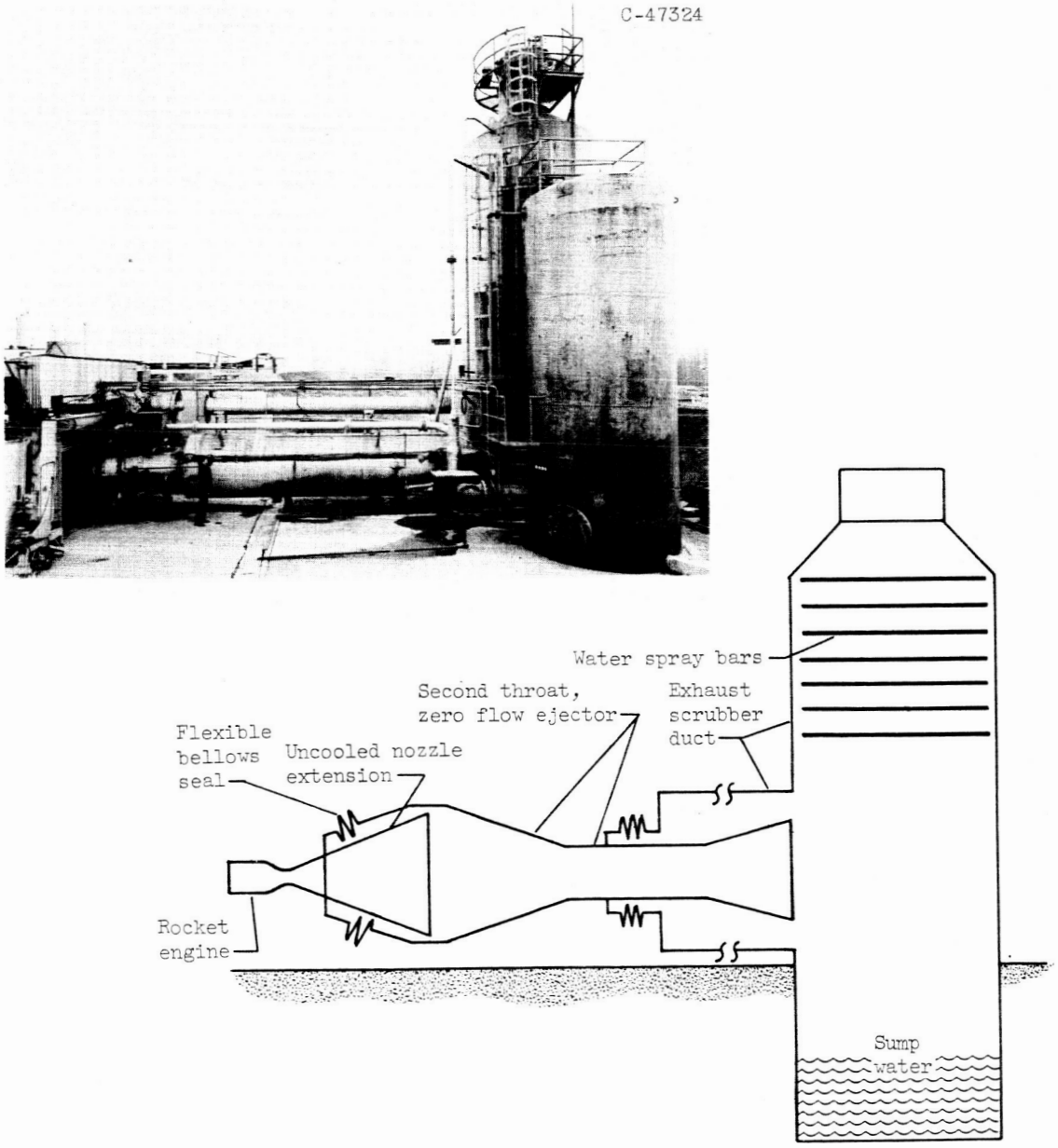

Figure 1. - General arrangement of rocket engine test facility.

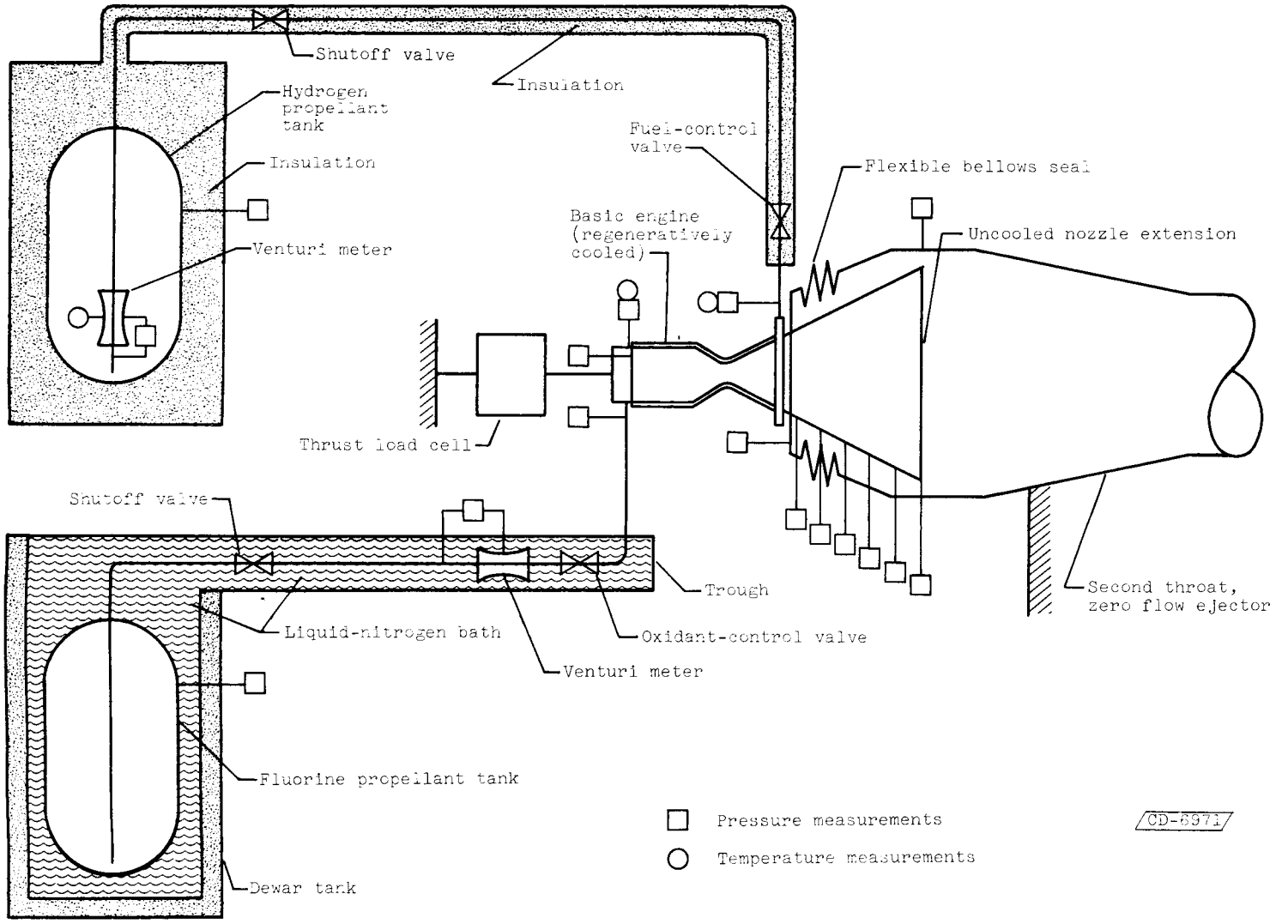

Figure 2. - Schematic diagram of engine and propellant system including instrumentation.

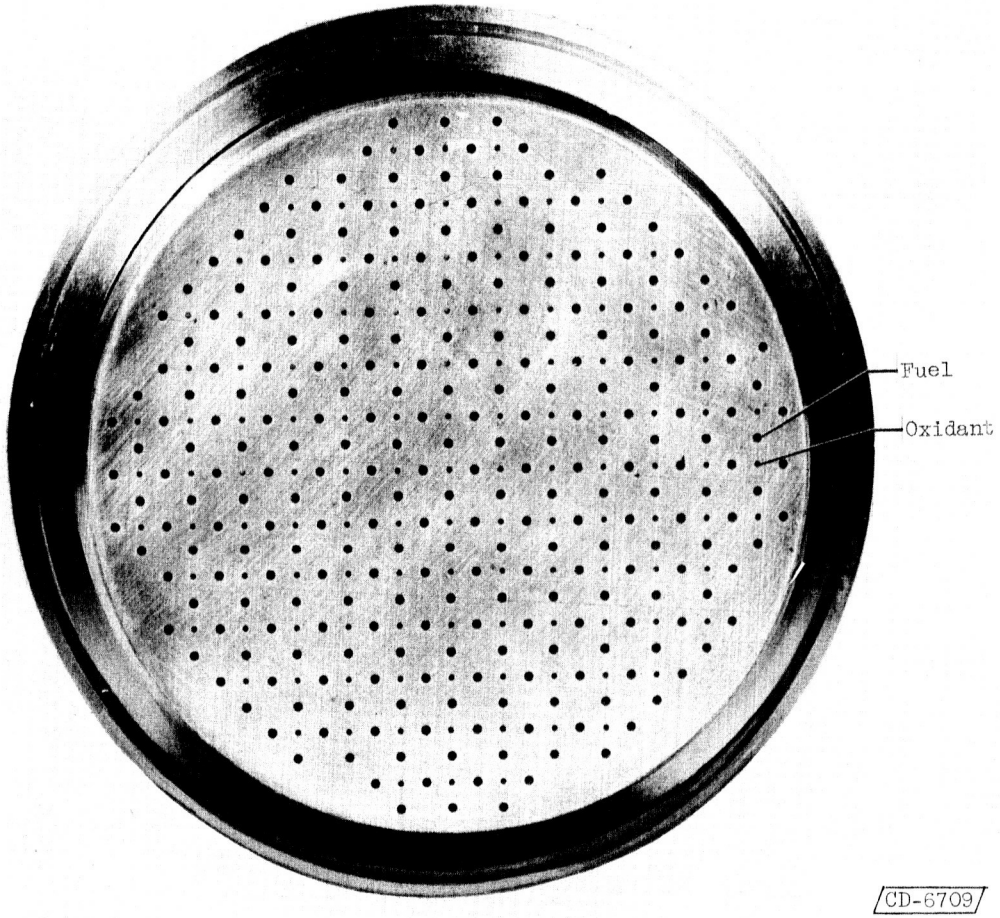

Showerhead

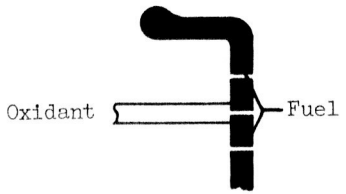

	Oxidant	Fuel
Number of holes	121	276 and 8
Hole diameter, in.	0.043	0.067 and 0.052
Total area, sq in.	0.176	0.990

Triplet

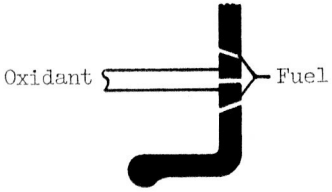

	Oxidant	Fuel
Number of holes	121	268
Hole diameter, in.	0.043	0.067
Total area, sq in.	0.176	0.945

(a) Showerhead and triplet.

Figure 3. - Injectors for 5000-pound-thrust engine.

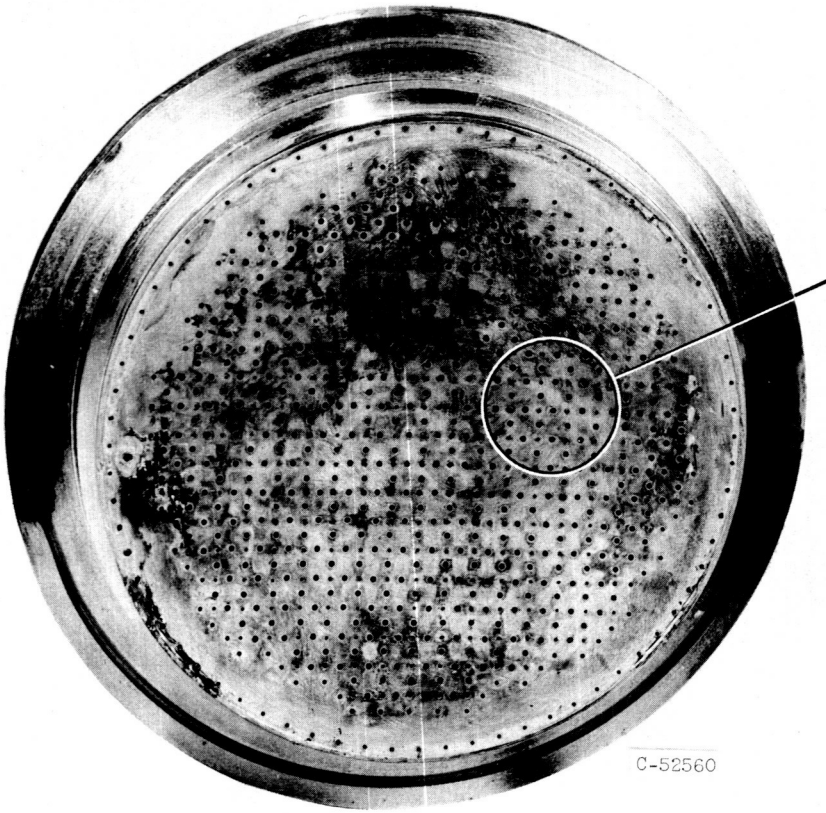

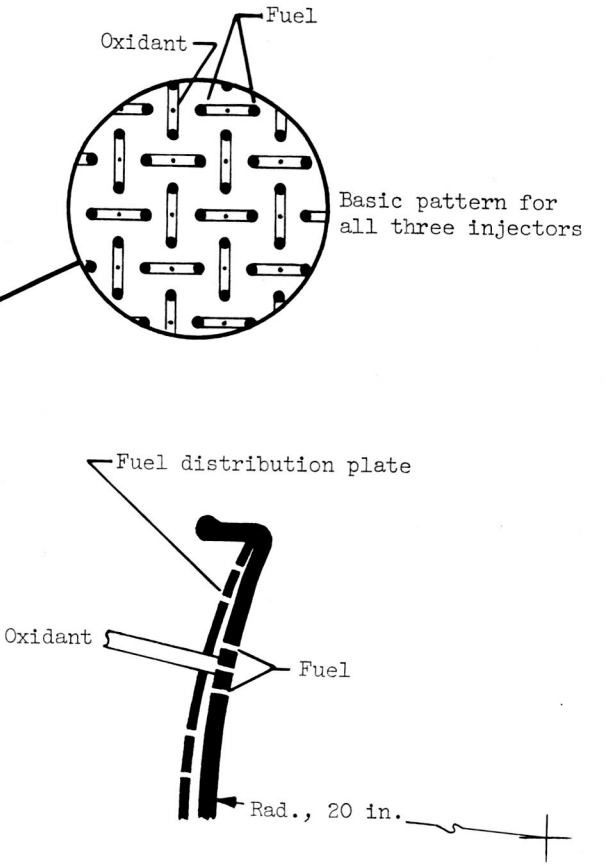

	Oxidant	Fuel
Number of holes	277	516, 76, and 72
Hole diameter, in.	0.041	0.052, 0.038, and 0.030
Total area, sq in.	0.365	1.224

CD-7016

(b) Converging showerhead.

Figure 3. - Concluded. Injectors for 5000-pound-thrust engine.

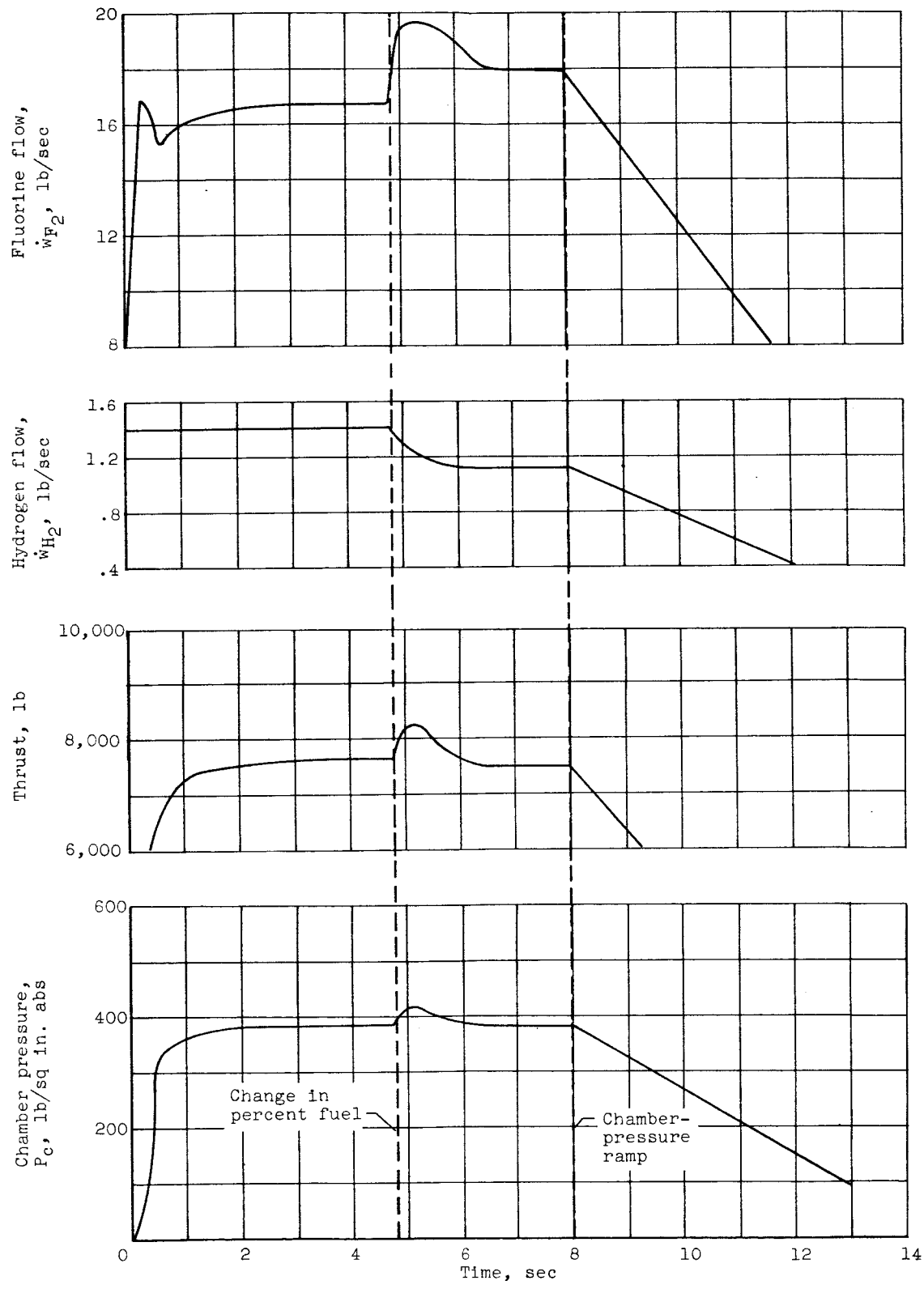

Figure 4. - Typical time history of engine performance run.

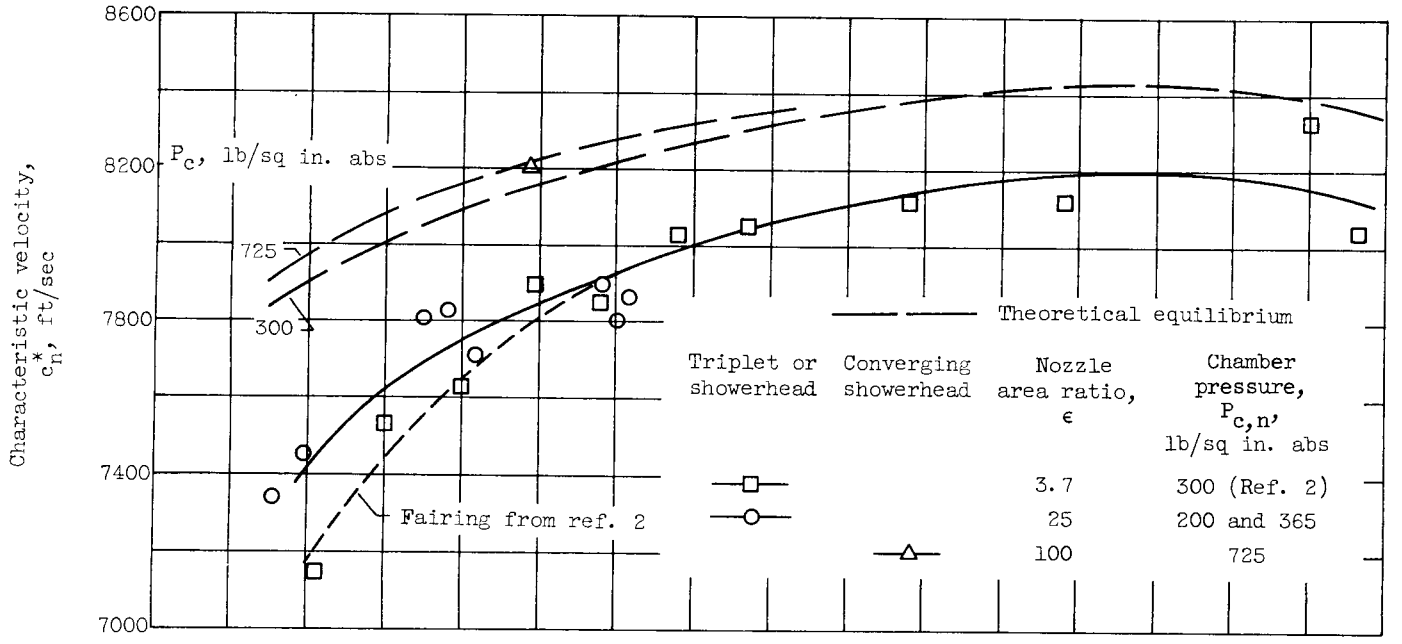

(a) Characteristic velocity.

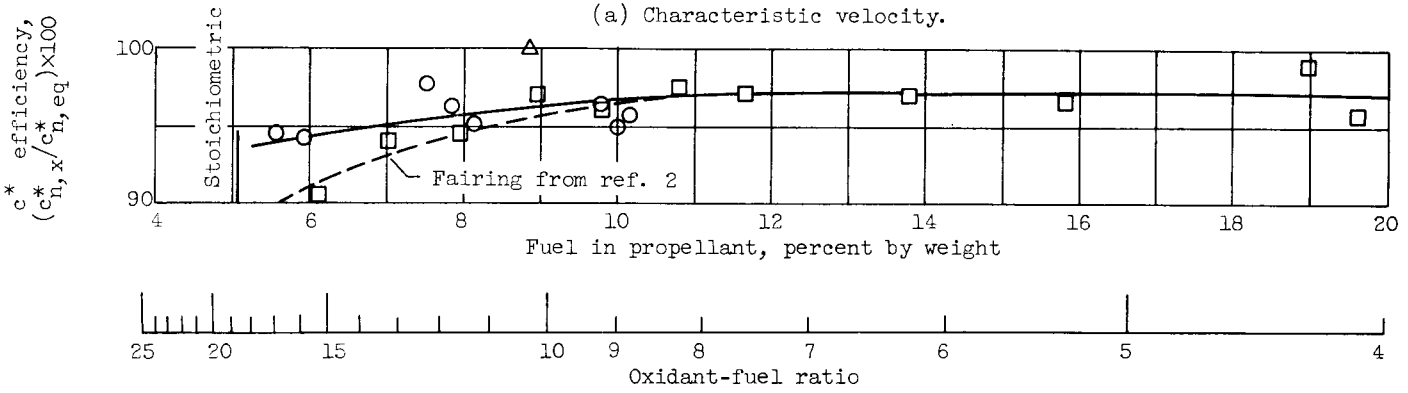

(b) Percent of theoretical equilibrium.

Figure 5. - Effect of variation of percent fuel on characteristic velocity.

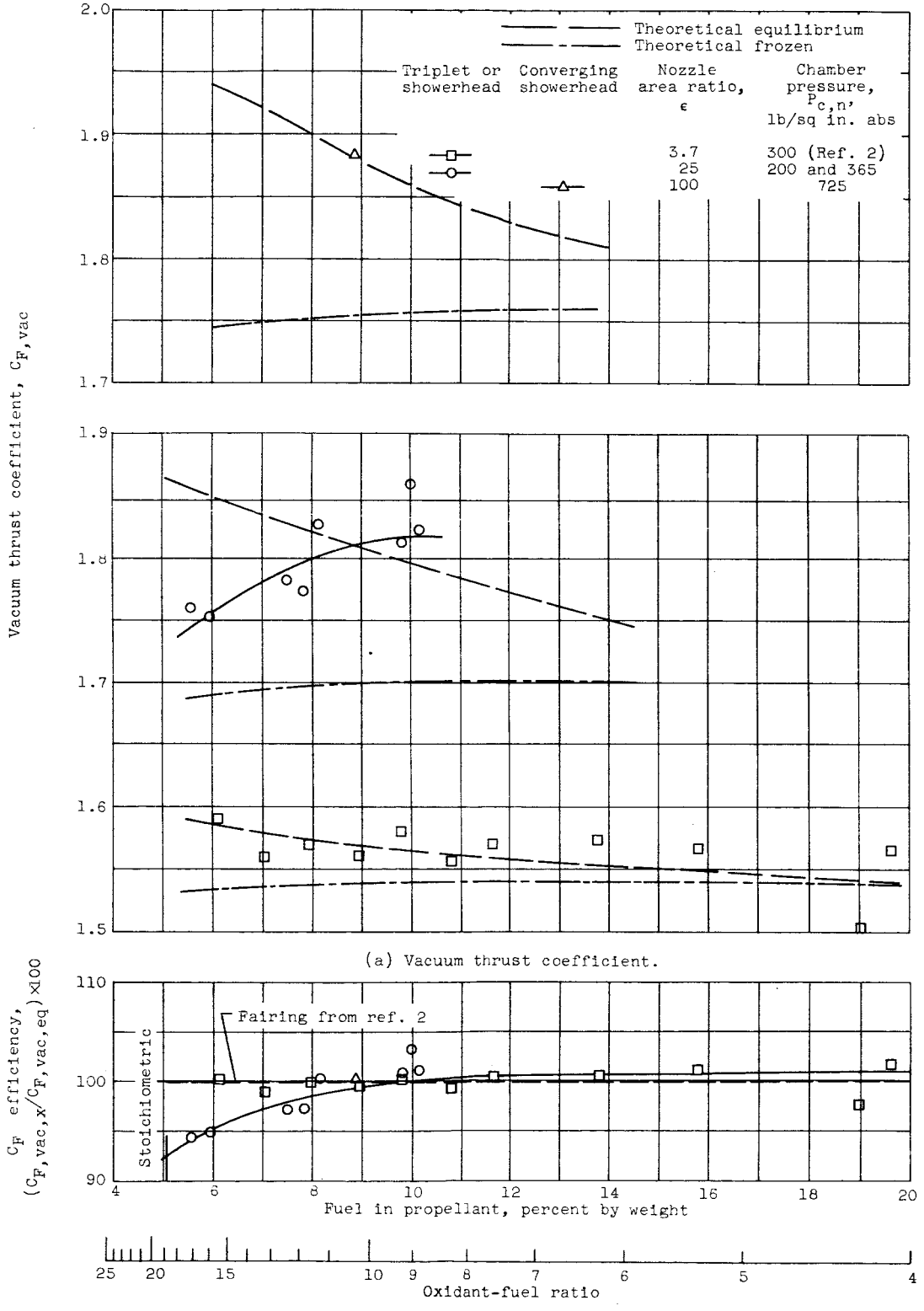

Figure 6. - Effect of variation of percent fuel on vacuum thrust coefficient.

[redacted]

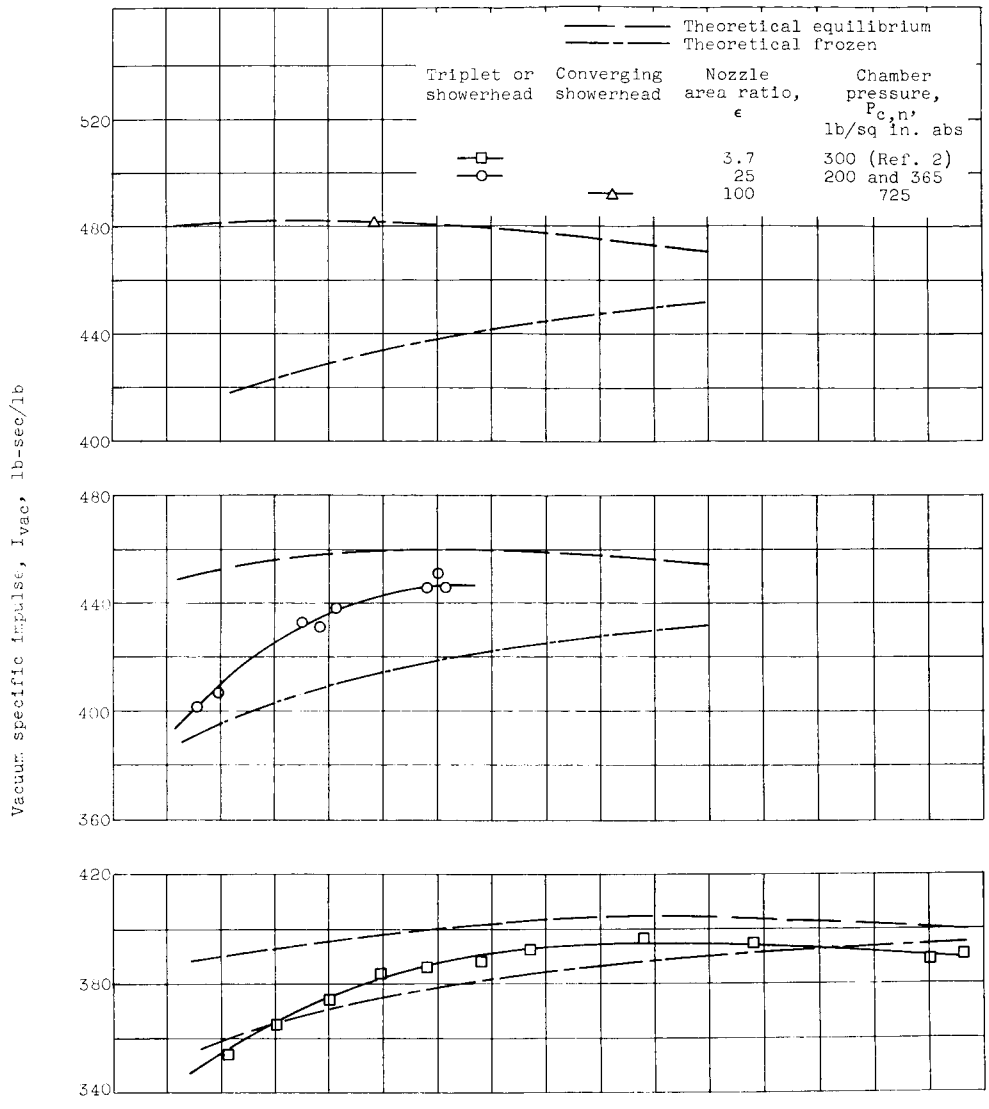

(a) Vacuum specific impulse.

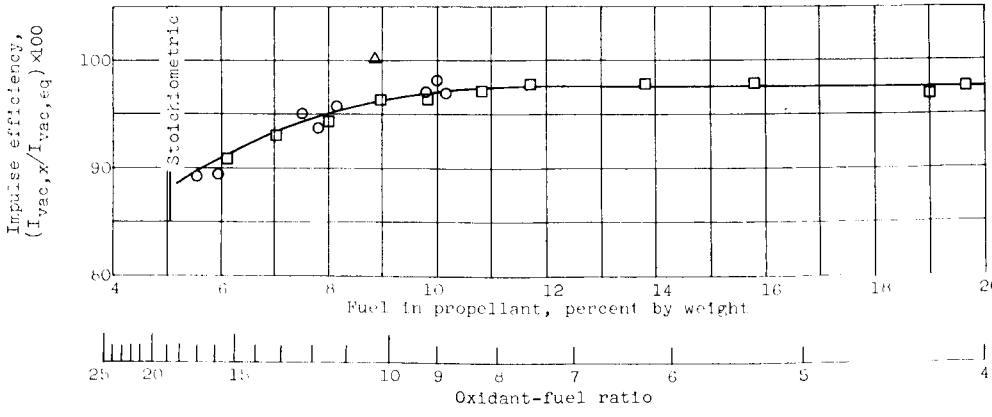

(b) Percent of theoretical equilibrium.

Figure 7. - Effect of variation of percent fuel on vacuum specific impulse.

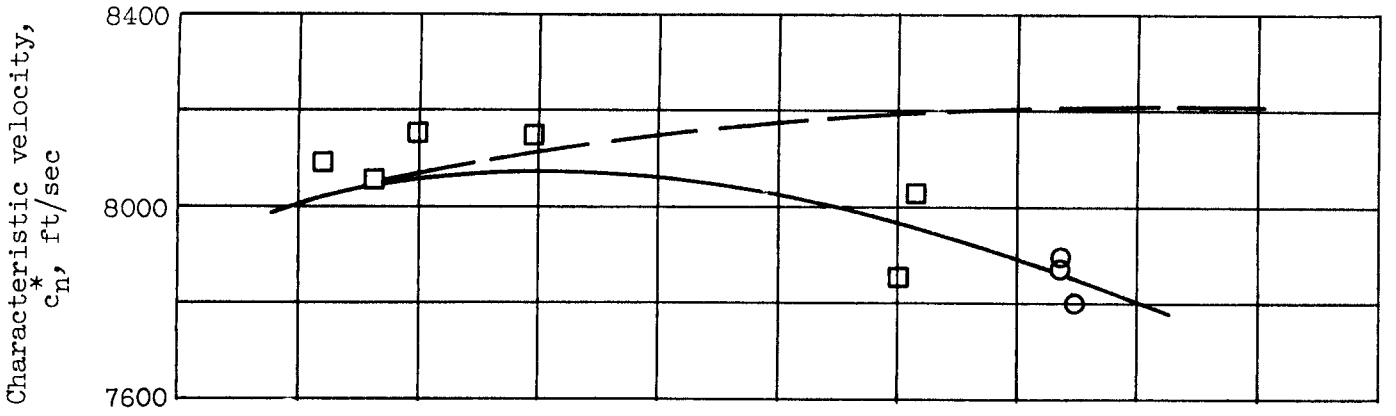

(a) Characteristic velocity.

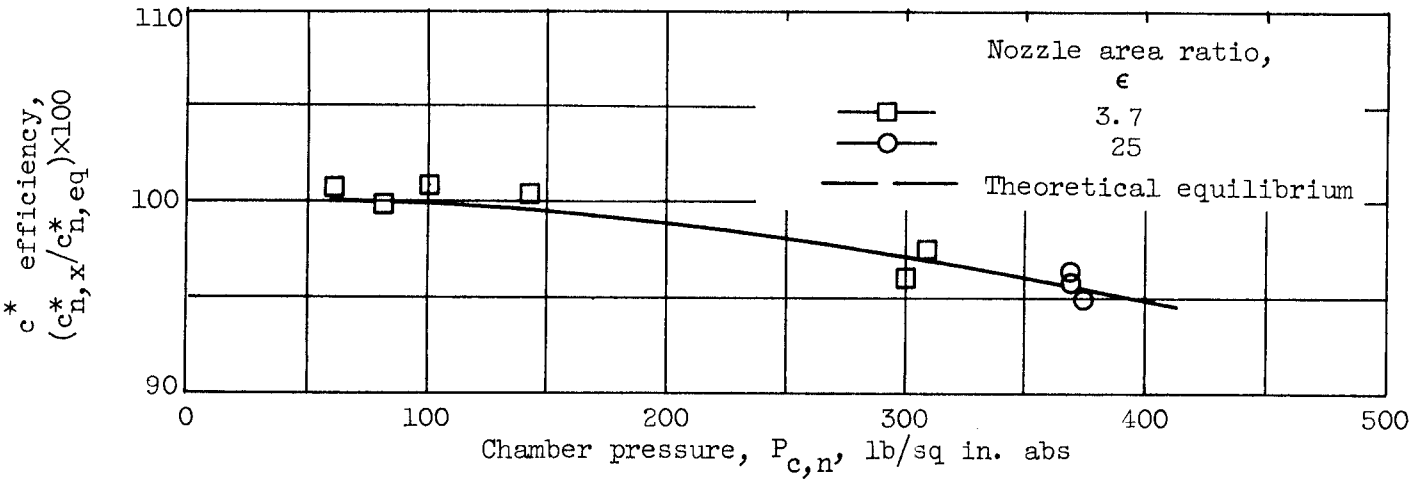

(b) Percent of theoretical equilibrium.

Figure 8. - Effect of chamber pressure on characteristic velocity at 10 percent fuel using showerhead injector.

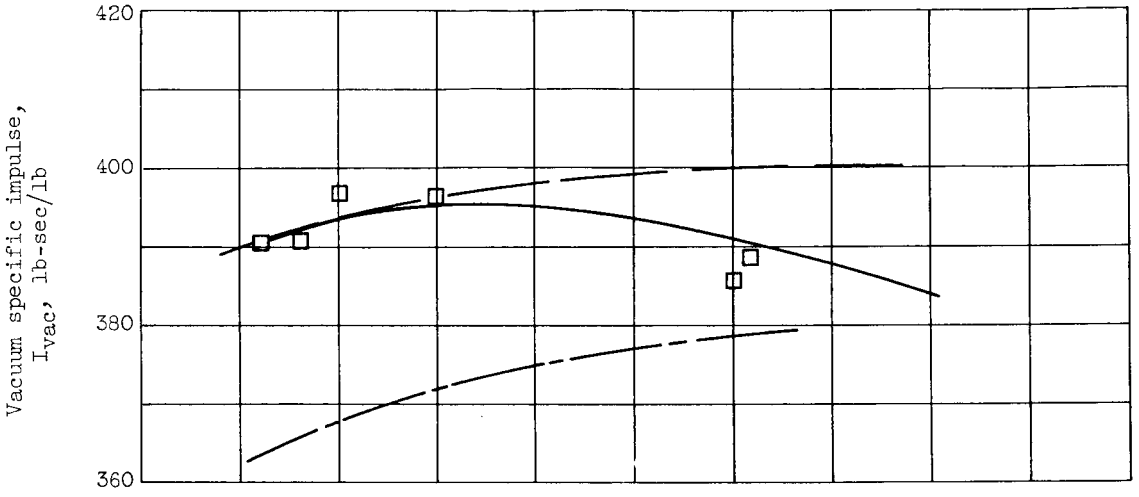

(a) Vacuum specific impulse.

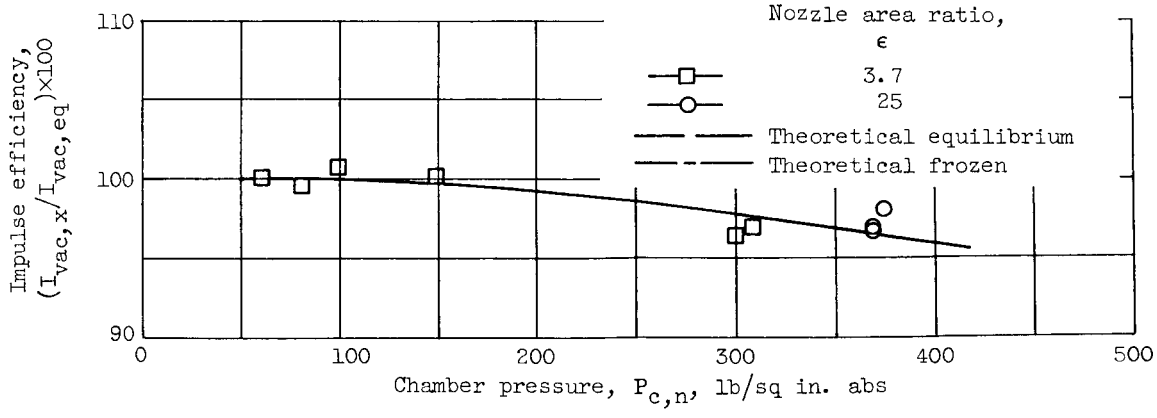

(b) Percent of theoretical equilibrium.

Figure 9. - Effect of chamber pressure on vacuum specific impulse at 10 percent fuel using showerhead injector.

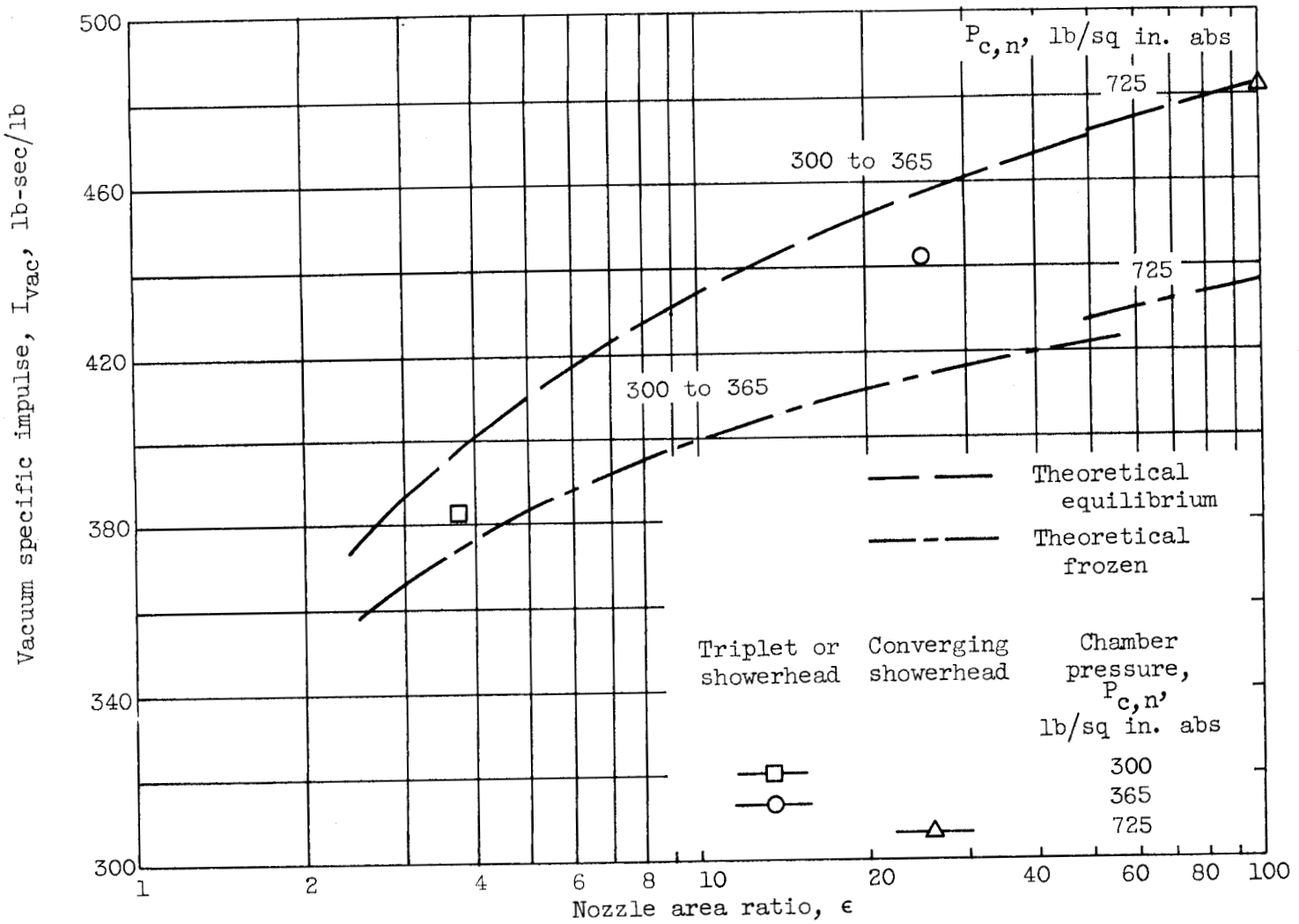

Figure 10. - Effect of nozzle area ratio on vacuum specific impulse at 9 percent fuel.

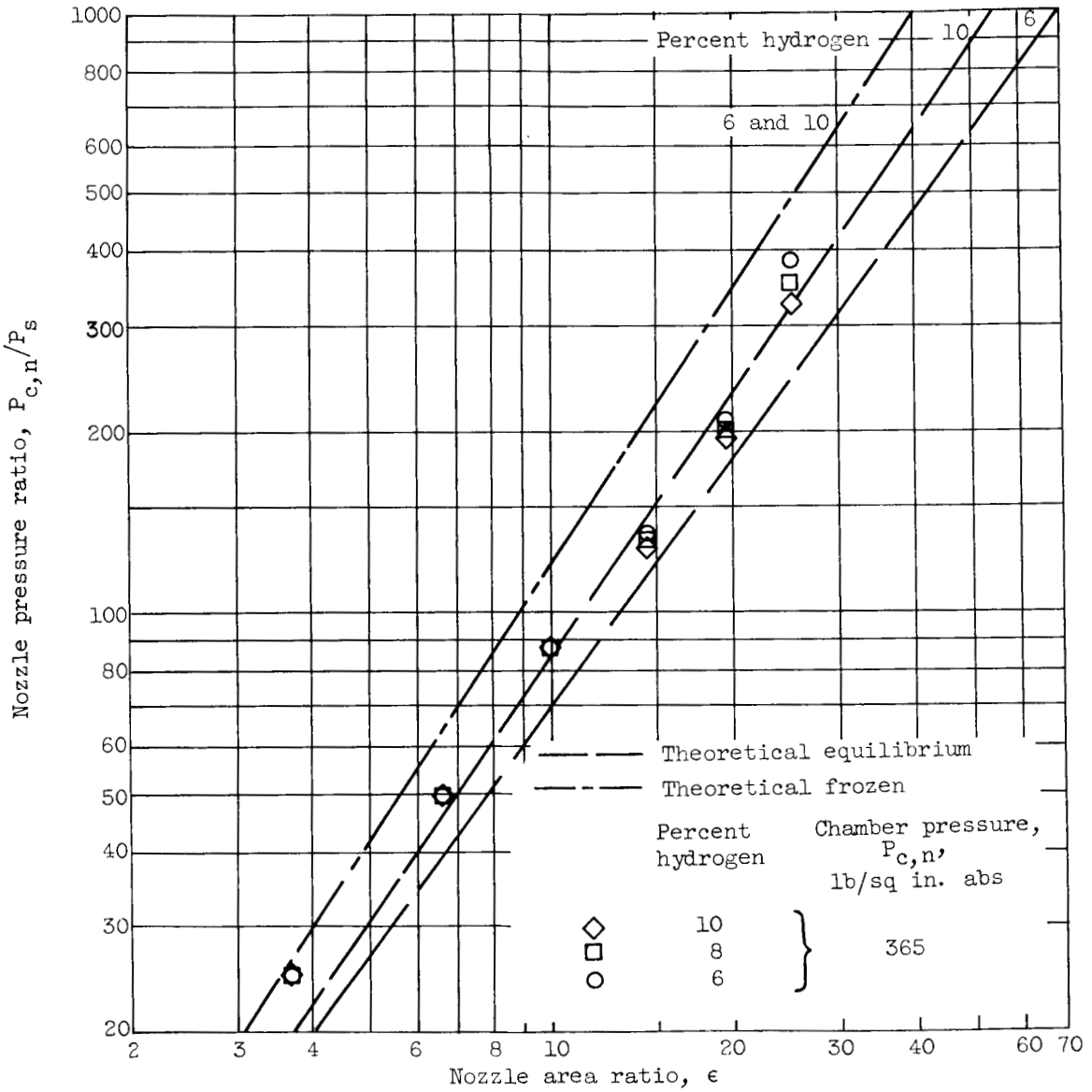

Figure 11. - Effect of nozzle area ratio on nozzle pressure ratio.

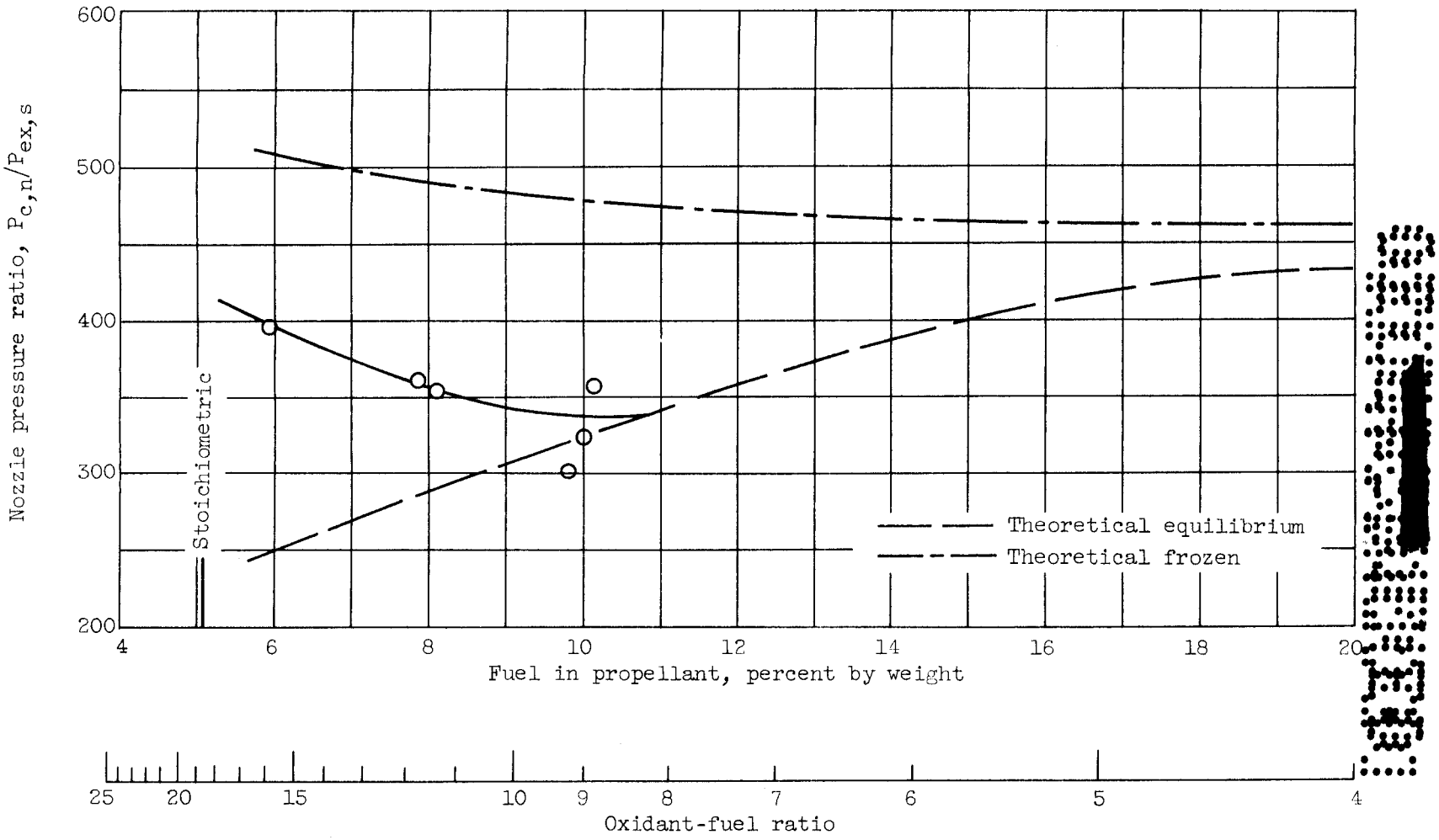

Figure 12. - Effect of mixture ratio on nozzle pressure ratio. Area ratio, 25:1; chamber pressure, 365 pounds per square inch absolute.

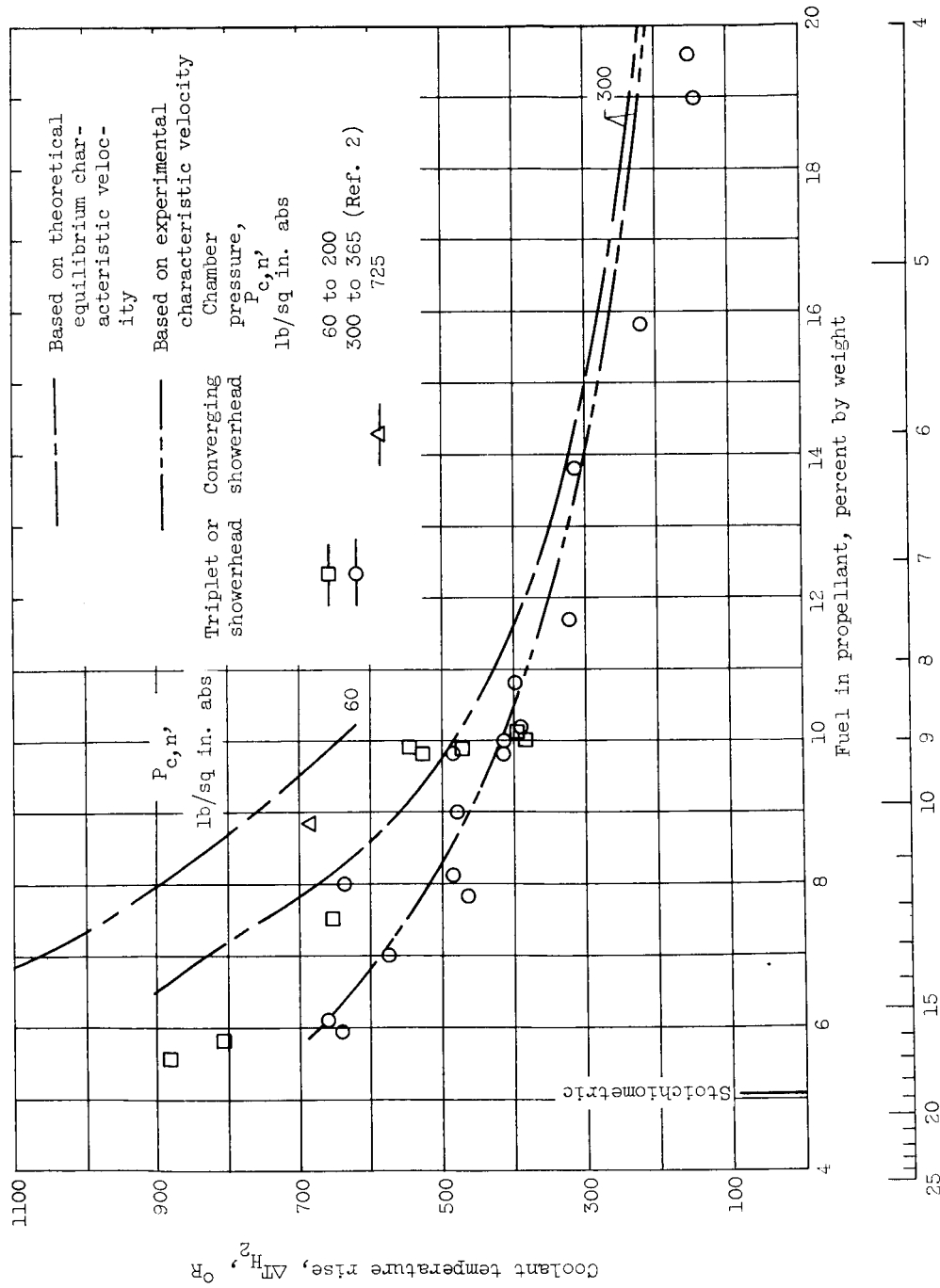

Figure 13. - Effect of mixture ratio on coolant temperature rise for regeneratively cooled 5000-pound-thrust rocket engine. Exhaust nozzle cooled to area ratio of 3.7; theoretical curves for engine designed for operation at 10 percent fuel and chamber pressure of 300 pounds per square inch absolute.